**NURETH14-134** 

# EXPERIMENTAL AND COMPUTATIONAL ANALYSIS OF STEAM CONDENSATION IN THE PRESENCE OF AIR AND HELIUM

M. Bucci<sup>1,2</sup>, W. Ambrosini<sup>1</sup>, N. Forgione<sup>1</sup>, F. Oriolo<sup>1</sup>, S. Paci<sup>1</sup>

University of Pisa, DIMNP, Largo Lucio Lazzarino 2, 56126 Pisa, Italy

CEA Saclay, CEA/DEN/DANS/DM2S/SFME/LETR, France

matteo.bucci@cea.fr

#### **Abstract**

Among the different phenomena expected to occur within nuclear reactor containments during a postulated loss of coolant accident, condensation on containment walls plays a major role, since it represents an important heat sink for evacuating the energy released by the discharge of the primary water. Nevertheless, condensation strongly affects other relevant phenomena, like containment atmosphere mixing, that influences the distribution of noncondensable gases hypothetically delivered in severe accident conditions. In this scenario, the role of condensation is not obvious, since it can locally aid the hydrogen produced by the oxidation of the core claddings to concentrate and reach flammability limits, providing a dangerous effect instead of a positive one. The understanding of condensation in the presence of air and hydrogen is therefore a fundamental task for the safety analyses of reactor containments. This research has been carried out with the aim to contribute to the understanding of these phenomena. A double strategy has been adopted, including complementary experimental and computational activities. Novel data have been made available by the CONAN facility, investigating the effects induced by light noncondensable gases in experimental configurations that were scarcely investigated in past studies. Computational fluid dynamics (CFD) condensation models have been developed and validated. The suitability of helium as a substitute for hydrogen in experimental activities has been investigated by theoretical and computational analyses allowing to establish simple criteria for the scaling of condensation tests in the presence of a light noncondensable gas.

## 1. Introduction

One of the main goals to be achieved by the adoption of CFD codes for containment safety analysis is the reduction of uncertainties and therefore an increase of confidence in the safe design of nuclear power plants. However, before a massive use of CFD codes can be considered advisable, the evidence of their reliability must be provided. In this aim, experimental data useful for the validation of these codes have to be produced. One of the most important benchmarks carried out in the field of condensation modelling in the last decades is probably the International Standard Problem 47 (ISP47) [1]. Analysing the results of the benchmark exercise, a general need was felt for achieving a better understanding of the effect of light noncondensable gases and improving the predictive capabilities of CFD models; in this purpose, smaller scale experimental analyses are advisable than those used for the ISP47. In this direction, research activities in the field of condensation modelling have been coordinated by University of Pisa and CEA in the frame of the SARnet network on severe accident (<a href="https://www.sar-net.eu">www.sar-net.eu</a>) [2-4]. Moreover, the separate effect CONAN facility operated by University of Pisa has been modified and

adopted to produce data on steam condensation in atmosphere of air and helium [5-7]. The aim of this paper is to summarize the main findings of these computational and experimental investigations, focusing on those aspects that can constitute the basis for further improvements in the understanding of condensation phenomena.

#### 2. CFD models

The set of balance equations characterizing the behaviour of a multicomponent mixture of steam, air and helium is given by the mixture continuity equation, species balance equations for two of the three species, the momentum balance equation and the thermodynamic energy balance equation:

• mixture continuity 
$$\frac{\partial \rho}{\partial t} + \nabla \cdot (\rho \mathbf{u}) = S_{m}$$
• steam 
$$\frac{\partial \rho_{v}}{\partial t} + \nabla \cdot (\rho_{v} \mathbf{u}) = -\nabla \cdot \mathbf{j}_{v} + S_{v}$$
• air 
$$\frac{\partial \rho_{a}}{\partial t} + \nabla \cdot (\rho_{a} \mathbf{u}) = -\nabla \cdot \mathbf{j}_{a} + S_{a}$$
• helium 
$$\frac{\partial \rho_{he}}{\partial t} + \nabla \cdot (\rho_{he} \mathbf{u}) = -\nabla \cdot \mathbf{j}_{he} + S_{he}$$
• momentum 
$$\frac{\partial \rho \mathbf{u}}{\partial t} + \nabla \cdot (\rho \mathbf{u} \mathbf{u}) = \nabla \cdot \mathbf{\tau} - \nabla P + \rho \mathbf{g} + \mathbf{S}_{q}$$
• thermodynamic energy 
$$\frac{\partial \rho e}{\partial t} + \nabla \cdot (\rho \mathbf{u} \mathbf{h}) = \nabla \cdot \left( k \nabla T - \sum_{k=v,a,he} \mathbf{j}_{k} h_{k} \right) + S_{h}$$

A common strategy for modeling wall condensation in CFD codes consists in assigning volumetric sinks in the cells adjacent to the condensing interface [2], as shown in Figure 1. Volumetric sources of mass, steam, energy and momentum are therefore implemented in the balance equations, respectively defined as

Overall Mass 
$$S_m = \dot{m}''_{v,i}/(2\Delta c)$$
 Steam  $S_v = S_m$   
Energy  $S_h = S_m h_{v,i}$  Momentum  $\mathbf{S}_q = S_m \mathbf{u}_c$ 

Moreover, the heat transfer through the condensing plate (if included in the computational domain) can be modelled by the conjugated heat transfer approach by assigning an appropriate source term to the solid cells contiguous to the condensing interface

Energy in the solid plate 
$$S_{h,p} = -S_m h_{lv,i}$$

In order to evaluate the condensation mass flux  $\dot{m}_{v,i}''$  and thus the sources, different approaches can be adopted. In this work, two models have been developed adopting different strategies and having different purposes. A brief description of them is given in the following paragraphs.

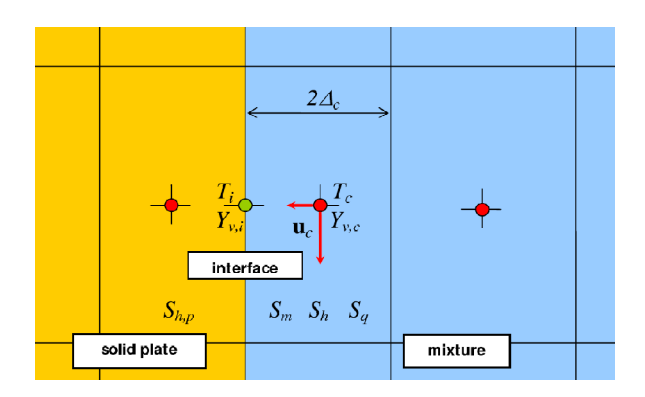


Figure 1 Sketch of discretization in the near- condensing-wall region.

## 2.1 The HMTDM (Heat & Mass Transfer Diffusion Method) model

This model is capable to evaluate the mass transfer rates on the basis of concentration distributions in the near wall region, without requiring any specific closure law; however, it requires a very fine space meshing since its accuracy depends on the concentration profiles next to the condensing wall. The condensation mass flux is calculated as

$$\dot{m}_{v,i}'' = \frac{\mathbf{j}_{v,i} \cdot \mathbf{n}_i}{1 - Y_{v,i}}$$

where  $\mathbf{n}_i$  is the normal to the condensing interface, pointing towards the fluid domain. The mechanistic character of the model consists in the way in which the diffusion fluxes are calculated. In this aim, two different models can be adapted: the effective binary diffusivity approximation and the full multispecies mass transfer model.

# 2.1.1 The HMTDM<sup>EBD</sup> model

Commercial CFD codes make often use of the so called equivalent binary diffusivity (EBD) approximation. According to the EBD approximation, the diffusion mass flux of a species is given by

$$\mathbf{j}_{k} = -\rho (D_{km} + D_{t}) \nabla Y_{k}$$

where the term  $D_{km}$  is the equivalent binary diffusivity of the species k in the mixture and  $D_t$  is the turbulent diffusivity, estimated according to the selected turbulence model. In CFD codes, like FLUENT, the equivalent binary diffusivity can be estimated by

$$D_{km} = \frac{1 - X_k}{\sum_{\substack{j=1\\j \neq k}} \frac{X_j}{D_{kj}}}$$

As shown by Bucci et al. [8], this formulation gives an appropriate description of diffusion for the condensing species, but not for noncondensable gases. Nevertheless, it is remarked that, according to this formulation, it is

$$\sum_{k=1}^{n} -\rho D_{km} \nabla Y_{k} \neq 0 \implies \sum_{k=1}^{n} \mathbf{j}_{k} \neq 0$$

A systematic error is therefore introduced in the balance equations of noncondensable species and in particular the species for which the balance equation is not solved but it is obtained summing the continuity equations and the balance equations of the other species. Indeed, when the details of molecular transport are dominant, as in the condensation boundary layer, the EBD approximation can lack of accuracy.

## 2.1.2 The HMTDM<sup>MSD</sup> model

To overwhelm the difficulties associated to the EBD model, an appropriate model is necessary, which can be deduced basing on the principles of irreversible thermodynamics as shown by Bucci [7], or basing on the kinetic theory of gases, as shown by Taylor and Kristhna [9]. The diffusion mass flux of the generic *k*-th species in a mixture of n species is given by

$$\mathbf{j}_{k} = -\rho \sum_{i=1}^{n-1} (\mathbf{D}_{kj} + D_{t} \delta_{kj}) \nabla Y_{j}$$

where  $D_{ki}$  are the terms of the multispecies diffusion matrix [D], given by

$$[D] = [A]^{-1}[R]$$

with

$$\mathbf{A}_{kk} = -M \left( \frac{X_k}{D_{kn} M_n} + \sum_{\substack{j=1 \ j \neq k}}^n \frac{X_j}{D_{kj} M_k} \right)$$

$$\mathbf{A}_{kj} = X_k M \left( \frac{1}{D_{kj} M_j} - \frac{1}{D_{kn} M_n} \right)$$

$$\mathbf{R}_{kk} = M \left( \frac{X_k}{M_n} + \frac{1 - X_k}{M_k} \right)$$

$$\mathbf{R}_{kj} = X_k M \left( \frac{1}{M_j} - \frac{1}{M_n} \right)$$

Due to its computational cost, the HMTDM model (mostly the MSD) is hardly applicable to large scale geometries. However, it is a very useful tool for achieving a better understanding of physical phenomena involved in condensation and relevant information for the development of coarser models for large scale analyses.

## 2.2 The HMTAM model (Heat & Mass Transfer Analogy Method)

This model estimates the condensation mass transfer rates on the basis of the heat and mass transfer analogy. The condensation mass flux is assigned as

$$\dot{m}_{v,i}'' = h_m \frac{Y_{v,i} - Y_{v,b}}{1 - Y_{v,i}} = h_m B_m$$

where  $h_m$  is the mass transfer coefficient and  $B_m$  is the condensation driving force. The mass transfer coefficient includes two terms

$$h_m = h_{m,0}F$$

that are the mass transfer coefficient at low mass transfer rates  $h_{m,0}$ , deduced on the basis of the heat and mass transfer analogy, and the correction factor of Stefan F, aimed at accounting for suction effects. Basing on the heat and mass transfer analogy, for low mass transfer rates, the Sherwood number is given by

$$Sh_{0,x} = Nu_{0,x} (Sc/Pr)^{1/3}$$

and the corresponding mass transfer coefficient by

$$h_{m,0} = Sh_{0,x} \frac{\rho D_{vm}}{x}$$

The condensation mass flux is therefore given by

$$\dot{m}_{v,i}'' = h_{m,0} F \frac{Y_{v,i} - Y_{v,b}}{1 - Y_{v,i}} = h_{m,0} \cdot \ln \frac{Y_{nc,b}}{Y_{nc,i}} = Sh_{0,x} \frac{\rho D_{vm}}{x} \cdot \ln \frac{Y_{nc,b}}{Y_{nc,i}}$$

The key point of the model is the choice of the appropriate correlation for the Nusselt number, which can be troublesome for complex geometries and not well defined phenomenology. On one hand, the Schlichting correlation [10] can be adopted for forced convection turbulent boundary layers:

$$Sh_{0,x,FC} = 0.0296 Re_x^{0.8} Sc^{0.33}$$

On the other hand, in natural convection boundary layers, the McAdams correlation [11] can be used:

$$Sh_{0.x.NC} = 0.13 Gr_x^{0.33} Sc^{0.33}$$

To deal with mixed convection effects, according to Incropera [11], the Sherwood number is estimated as

$$Sh_{0,x,MC}^{n} = \left| Sh_{0,x,FC}^{n} \pm Sh_{0,x,NC}^{n} \right|$$

where n is taken equal to 3. The sign + is used in *buoyancy opposed* conditions (gravity and inertia terms have different directions), whereas the sign – is used in *buoyancy aided* conditions [12]. Despite of the difficulties associated to the choice of the appropriate correlation, since the use of relative coarse meshing is possible, a significant reduction of computational resources is achieved, making this model applicable to large scale or even to full containment scale analyses.

## 2.3 Turbulence effects

The RNG  $\kappa-\varepsilon$  model is used to account for turbulence effects with both condensation models. Anyway, a different approach is used to deal with the near-wall turbulence. On one hand, the HMTDM models require a very fine meshing in the region near the condensing wall, since the accuracy of the condensation models relies on the capability to estimate temperature and concentration gradients in the condensing boundary layer. For this reasons, appropriate low Reynolds functions are adopted, which are referred to as Enhanced Wall Treatment (EWT) in the FLUENT code [13]. On the other hand, the HMTAM model allows adopting a relatively coarse discretization in the near-wall region. Standard logarithmic wall functions are thus used, even if not purposely conceived to deal with transpirating boundary layers.

Despite the use of the RNG  $\kappa - \varepsilon$  model, other choices are possible. Bucci et al. [14] and separately Bucci [7] investigated this possibility and concluded that the most turbulence models with low Reynolds capabilities are able to describe the qualitative behaviour of transpirating boundary layers.

## 3. Experiments and Computations

Two main physical properties differentiate a noncondensable light gas and air: molecular diffusivity and molecular weight. In the aim to investigate the effect of helium on steam condensation, the analysis has been thus divided into two parts: forced convection condensation, focusing on the effect of diffusivity, and natural convection condensation, combining both diffusivity and buoyancy effects. Two different experimental campaigns and computations have

been carried out with a multiple purpose: qualify experimental data, validate CFD models and achieve information on the involved phenomena.

## 3.1 Main features of the CONAN facility

The CONAN facility (CONdensation with Aerosols and Noncondensable gases) is operated by the Department of Mechanical, Nuclear and Production Engineering of the University of Pisa. The facility consists of three different loops, primary, secondary and tertiary (see Figure 2), which accomplish with the operating needs encountered in running the experiments:

- the primary loop, in which the mixture of steam and noncondensable gases circulates and partly condenses on a flat wall;
- the secondary loop, which provides the required cooling of the condensing plate by circulating water, whose temperature can be varied;
- the tertiary loop, which allows controlling the temperature of the cooling fluid (the water of the secondary loop).

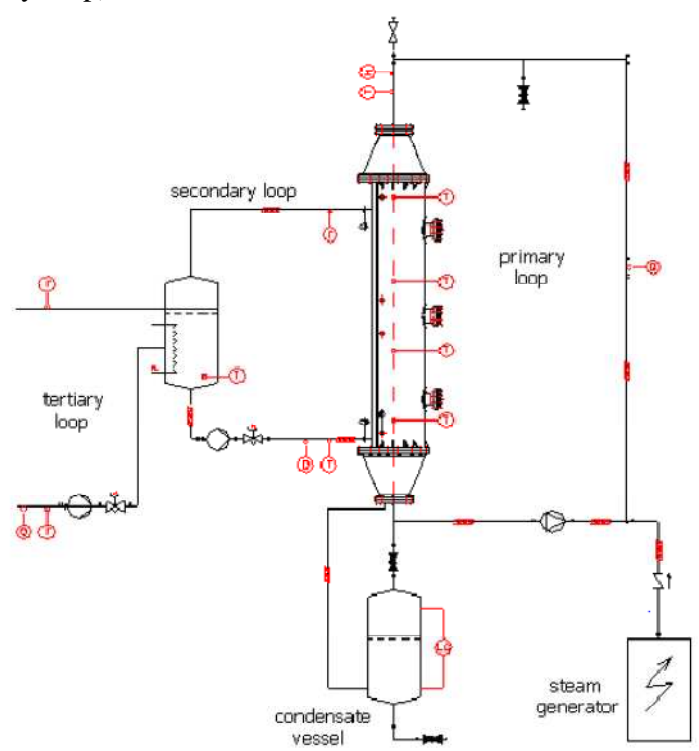


Figure 2 Layout of the CONAN facility.

The primary loop contains the test section (see Figure 3), consisting in a roughly 2 m long, 0.34 m side channel having square cross section, in which a mixture of steam, air and helium is circulated in downward flow. One of the lateral surfaces of the channel belongs to a 4.5 cm thick aluminium flat plate, cooled on the back side by the water of the secondary loop. Condensation occurs on the inner surface of the cooled plate and the related condensate flow is collected at the bottom of it by a gutter and routed by a small diameter piping to an external vessel; a relatively accurate estimation of the condensate flow is obtained by differential pressure measurement in this vessel (the uncertainty on the overall condensation rate is  $\pm 1\%$ ). Moreover, local temperature measurements are available at different locations and depths along and in the

thickness of the aluminium plate where condensation occurs, permitting to estimate local heat fluxes (with an uncertainty of  $\pm 700$  W), on whose bases the local mass fluxes are deduced. The other surfaces of the test section are insulated from the external environment, to avoid that condensation occurs over them. Variable area sections connect both the test section channel to the primary loop piping. The bottom part of the test section is connected to a variable speed blower for circulating the gas mixture. Steam produced by an electrical steam generator, with a nominal power of 60 kW, is injected in the bottom part of the primary loop via a tee junction. The uppermost part of the primary loop is presently connected to the external atmosphere via an open pipe, to maintain atmospheric pressure conditions.

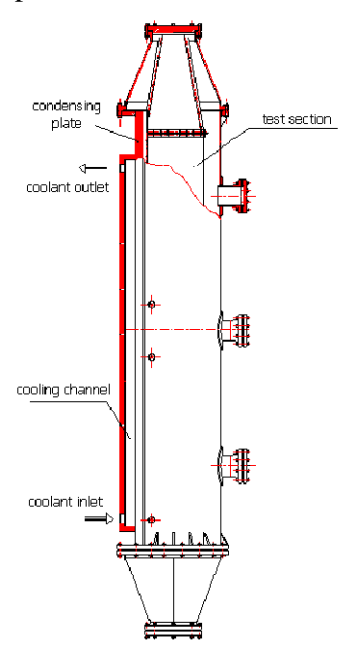


Figure 3 Test section of the CONAN facility.

To accomplish with the objective of the present research, tests have been performed having different steam generator power (from 5 to 25 kW), different mixture velocity (from 0.5 to 3.5 m/s) and relative concentrations of the noncondensable gases (from 0% to 100% of helium in the noncondensable mixture).

#### 3.2 Forced convection

A useful way for analysing experimental results consists in comparing local experimental Sherwood numbers deduced by measurements to those predicted by the analogy adopting an appropriate correlation, that in turbulent forced convection can be the Schlichting's.

Basing on temperature measurements within the condensing plate, the local condensation mass fluxes can be deduced. The experimental local Sherwood number is therefore estimated as

$$Sh_{0,x} = \frac{\dot{m}'' x}{\rho D_{vm}} \cdot \left( \ln \frac{Y_{nc,b}}{Y_{nc,i}} \right)^{-1}$$

In Figure 4 the results of this analysis are shown for tests at 20 kW. In forced convection conditions, a remarkable agreement is obtained for Reynolds number higher than 10<sup>5</sup>. As a

matter of fact, for fully developed forced convection condensation the analogy is capable to provide an appropriate description of heat and mass transfer phenomena.

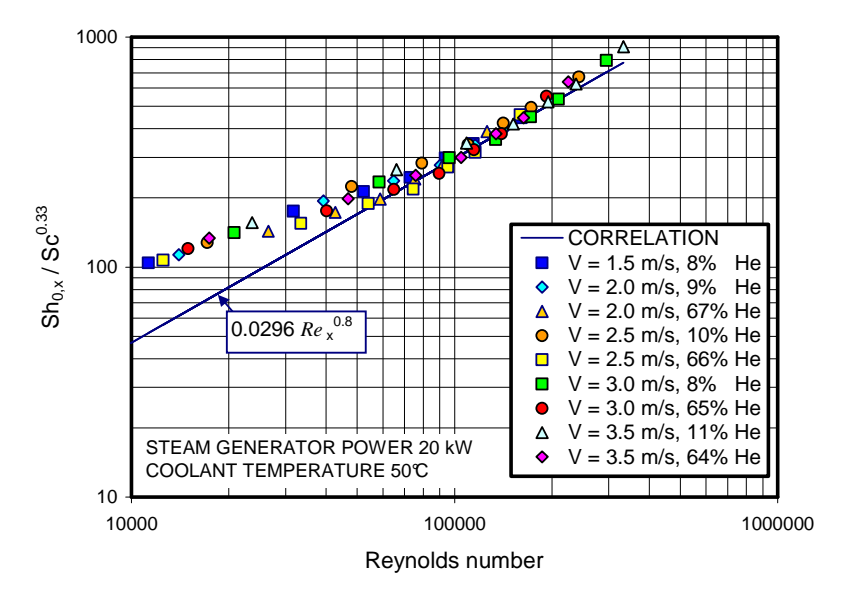


Figure 4 Experimental Sherwood number in forced convection condensation tests at 20 kW.

Relevant information provided by the analogy and confirmed by experiments (see Figure 5) is also that, for a given inlet velocity and a given steam generator power, helium concentration has a minor effect on the overall condensation rate. The increase of the steam diffusivity and the condensation driving forces are in fact counterbalanced by a reduction of the mixture density, which implies a decrease of the maximum attainable Reynolds and Sherwood numbers. As result, the condensation rate does not change noticeably with helium.

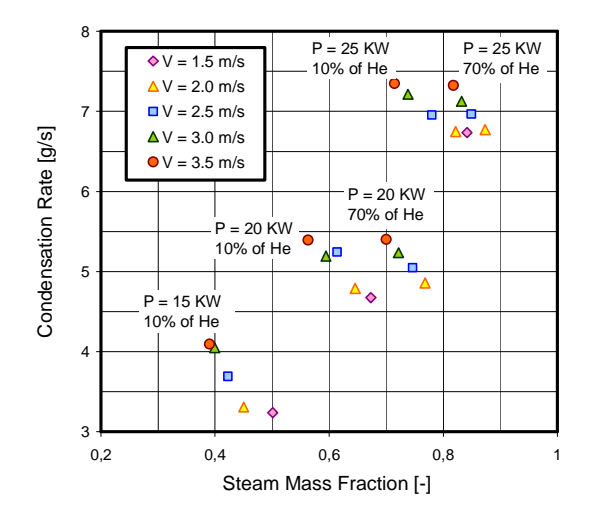


Figure 5 Overall condensation rates in forced convection condensation tests.

## 3.3 Buoyancy effects

In condensing mixtures of steam and air, the fluid close to the interface is heavier than in bulk, since the condensing interface is cold and rich of air. Natural convection regimes are established if buoyancy forces are strong enough to overwhelm inertia forces. In the presence of large quantities of helium, however, the non-equilibrium between interface and bulk density can be reduced. For certain helium concentrations the density difference can be even annealed and forced convection regimes can be thus experienced even at low velocities. This phenomenon has been observed in CONAN tests with helium concentrations in bulk to about 62% (see Figure 6).

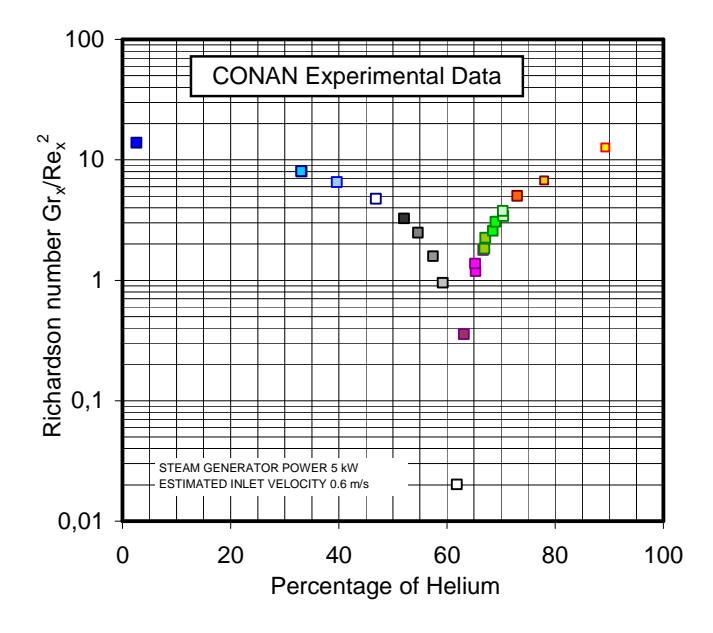


Figure 6 Richardson number in condensation tests at low velocity.

While for low concentrations of helium a natural convection regime is experienced (see Figure 7, blue dashed line), for tests at high helium concentration (around 60%), the comparison between experimental asymptotic Sherwood numbers and correlations for forced (Schlichting) and natural (McAdams) convection pointed out the presence of a forced convection regime (black dashed line). The transition between the steam-air natural convection regime and the steam-air-helium mixture convection regime is investigated in Figure 8 (left). Experiments and computations confirm a progressive reduction of the Sherwood number from 0% to 60% of helium, due to a reduction of buoyancy forces. However, the most interesting phenomena have been observed with helium concentrations larger than 62%, for which an inverse density gradient establishes, since the density at the interface is lower than the bulk one. This phenomenon has been called buoyancy reversal, in which buoyancy and inertia forces act in opposite directions. If reversed buoyancy forces are strong enough, a local inversion of the velocity field can be experienced. This phenomenon, named *flow reversal*, is clearly reproduced by the HMTDM models, e.g., for tests at 90% of helium (see Figure 8, right), but experimental data suggest its presence also for tests at lower concentrations (see Figure 8, left). Indeed, the phenomenon is associated to a sharp increase of the mass transfer coefficient and the condensation rate. As shown in Figure 7, a natural convection regime establishes with improved mass transfer characteristics (red dashed line). Detailed computations show that the occurrence of buoyancy reversal and the subsequent flow reversal involves a significant increase in turbulence in the near-wall region, which is suggested as the cause of improved mass transfer with respect to steam-air natural convection.

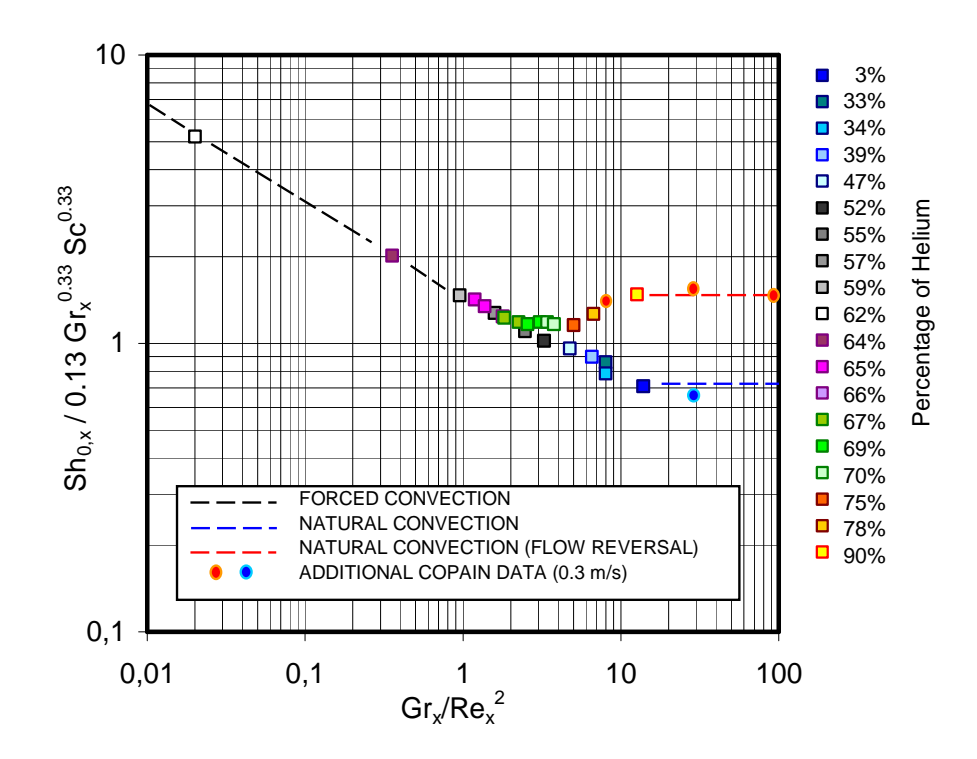


Figure 7 Experimental Sherwood number in condensation tests at low velocity.

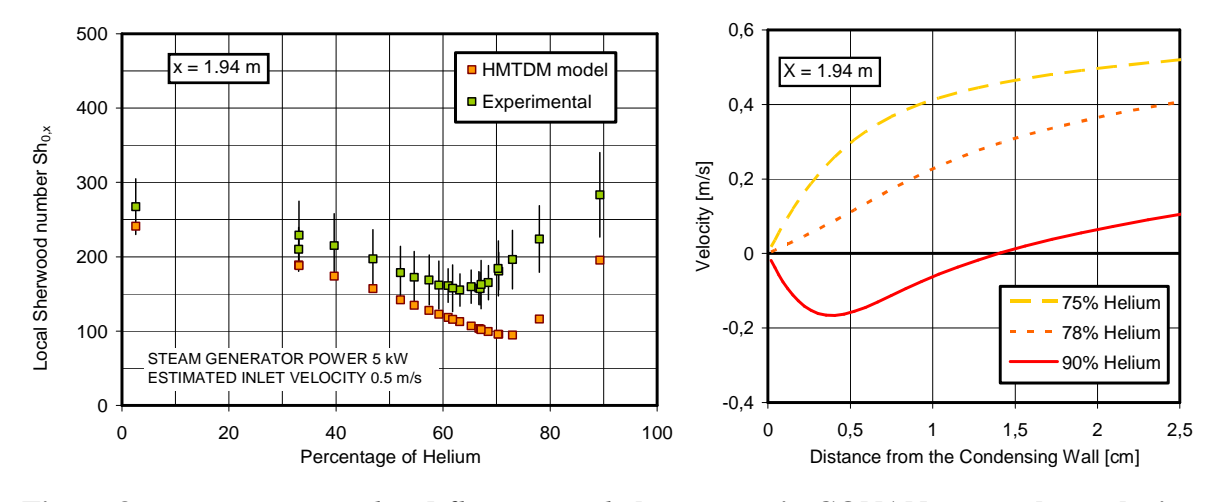


Figure 8 Buoyancy reversal and flow reversal phenomena in CONAN tests at low velocity.

## 3.4 Results of computations

Computations have been performed with the FLUENT code, where the three different condensation models have been implemented. Turbulence effects have been modelled with the

RNG  $\kappa - \varepsilon$  model. To deal with near-wall turbulence the FLUENT Enhanced Wall Treatment was used with the HMTDM models (EBD and MSD), whereas standard logarithmic wall functions have been used with the HMTAM model. An overview on the performance of condensation models is given in Figure 9, where the overall condensation rates calculated by the three models are compared to the experimental ones. The overall behaviour of the models is satisfactory for both forced convection and low velocity cases. A relatively poorer prediction of local heat and mass transfer rates has been ascertained in the entrance region (see Figure 10 and Figure 11), which could have caused a slight underestimation of overall condensation rates. Indeed, even if the asymptotic behaviour of local heat fluxes is correctly reproduced, a lack of accuracy affects the description of the developing region next to the inlet section, for which the selected turbulence models are less appropriate. Important information deduced by analysing local heat fluxes is also that, in turbulent forced convection condensation, only minor differences must be expected between the EBD and the MSD model: as expected, the more important is turbulent diffusion, the more similar are results obtained by the two formulations. Last but not least, it is worthy of consideration the trend of local heat flux predicted by the EBD and the MSD model for the case at low velocity and rich of helium (see Figure 11, right). Near the outlet section of the channel a sharp increase of the experimental heat flux is ascertained, reproduced correctly by the HMTDM models. This phenomenon is attributed to the presence of flow reversal, as shown in Figure 8 (right).

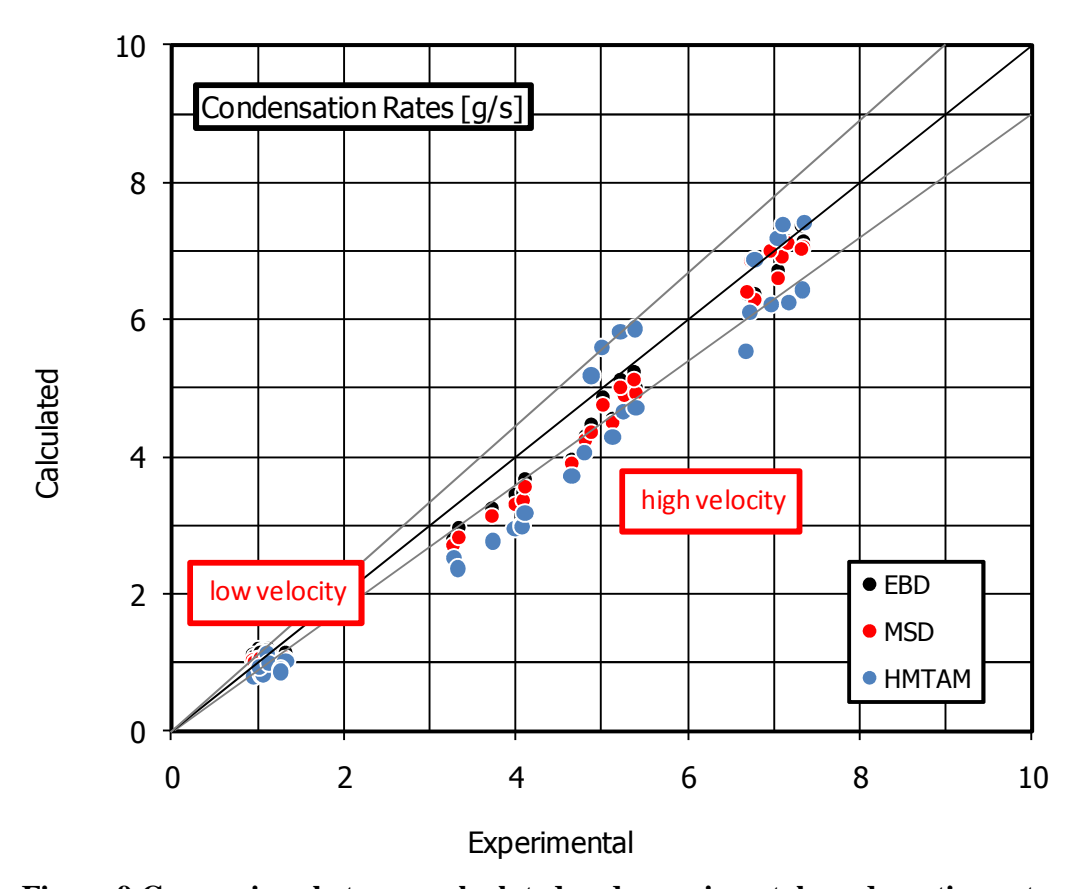


Figure 9 Comparison between calculated and experimental condensation rates.

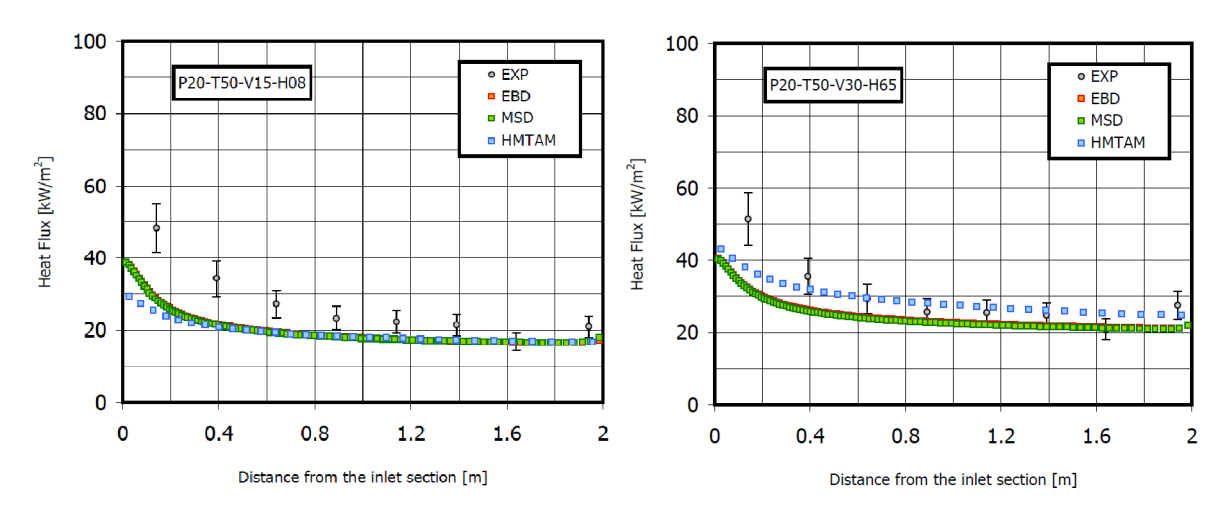


Figure 10 Comparison between calculated and experimental heat fluxes (high velocity).

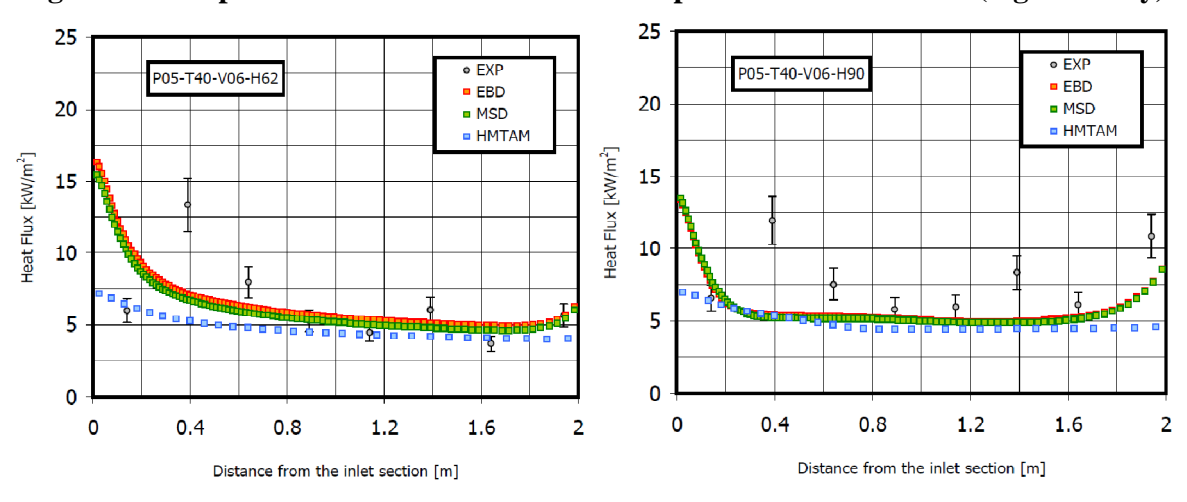


Figure 11 Comparison between calculated and experimental heat fluxes (low velocity).

## 4. Scaling of condensation tests for hydrogen safety analyses

Basing on the molar formulation of the heat and mass transfer analogy, simple scaling criteria can be found, estimating the ratio of the local condensation rates for mixtures of steam-air-hydrogen and steam-air-helium having equivalent molar concentration [7,15]. As in the previous analyses, the cases of forced convection and low velocity have to be treated separately.

#### 4.1 Scaling of forced convection tests

Basing on the Schlichting correlation, in forced convection conditions, for a given mixture inlet velocity and temperature boundary conditions, this ratio can expressed as [7]

$$R_{FC} = \frac{\dot{m}_{v,i}''(h_2)}{\dot{m}_{v,i}''(he)} = \left(\frac{D_{vm}(h_2)}{D_{vm}(he)}\right)^{2/3} \left(\frac{\rho(h_2)}{\rho(he)}\right)^{7/15} \left(\frac{\mu(h_2)}{\mu(he)}\right)^{-7/15}$$

A scaling criterion can be thus established simply basing on film properties, which are the properties of the mixture evaluated at the average temperature between the bulk and the

condensing interface. The quantity  $R_{FC}$  can be plotted in triangular diagrams where the three axes represent the molar fractions of the three species (see Figure 12). Moreover, since steam is considered in saturation conditions, as in actual CONAN tests, if the mixture is assumed to behave as an ideal gas mixture, the steam molar fraction can be occasionally replaced by the steam saturation temperature corresponding to its partial pressure. As a consequence the lines representing constant steam mass fraction are also at constant temperature.

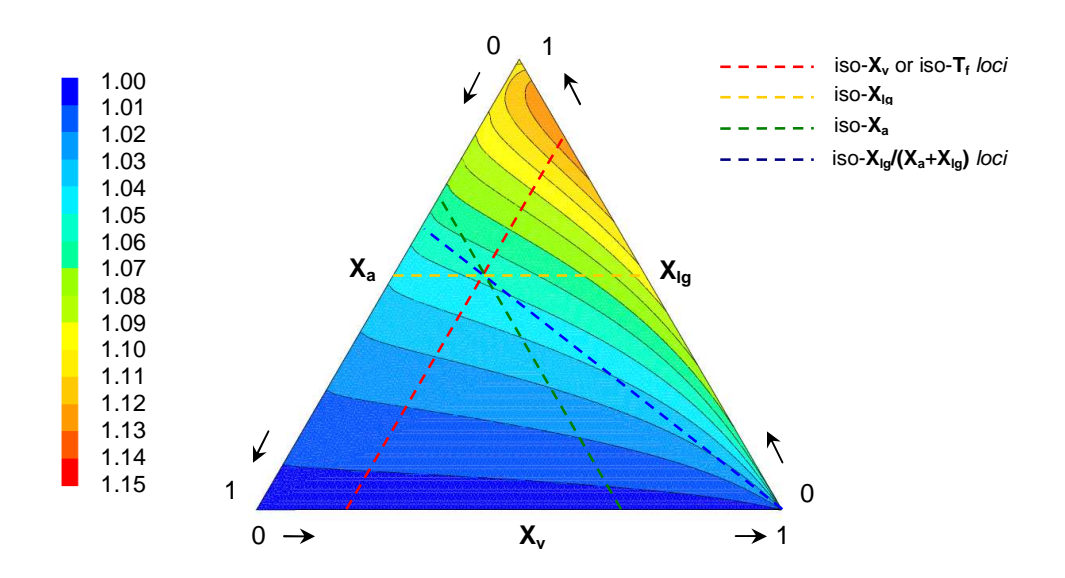


Figure 12  $R_{FC}$  at atmospheric pressure

The theoretical correlation proposed above has been tested against the prediction of the MSD model, proving the consistency of the analysis. For the sake of simplicity a single case having 30 °C of condensation temperature and 90 °C of bulk (inlet) temperature is considered. The line identifying the intersection of  $R_{FC}$  with the steam molar fraction corresponding to a film temperature (60 °C) is reported in Figure 13 (red dashed line). In the same figure, the values predicted by CFD computations performed with the MSD model are reported. The results of this analysis allow to conclude that mixtures of hydrogen and helium having the same molar concentrations give similar mass fluxes in forced convection.

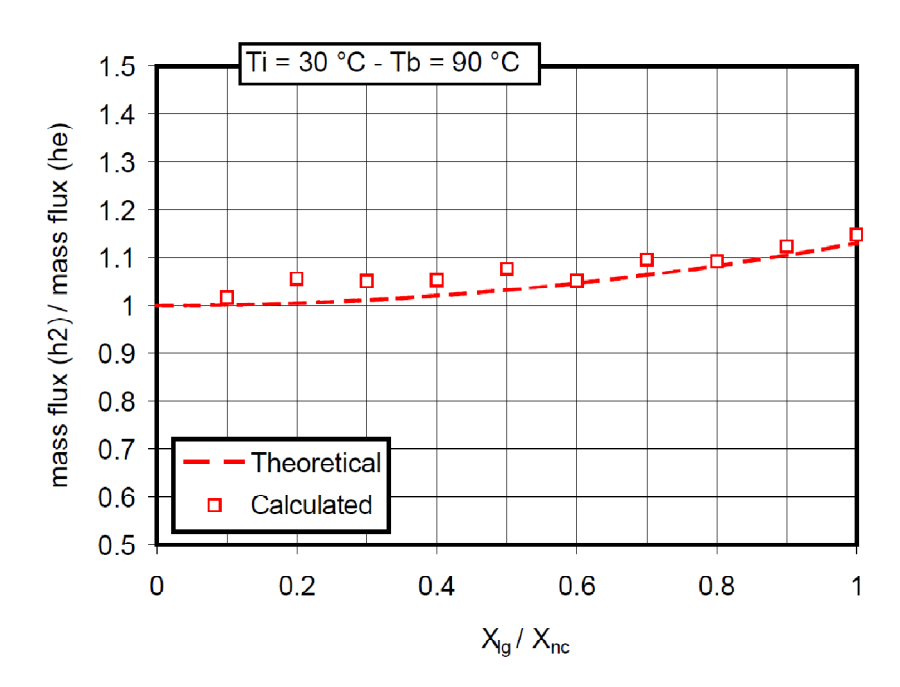


Figure 13 Comparison of theoretical and calculated  $R_{FC}$  at atmospheric pressure and 60 °C of film temperature

## 4.2 Scaling of low velocity tests

Contrarily to forced convection, in the presence of buoyancy forces, the ratio of the local condensation rates for mixtures of steam-air-hydrogen and steam-air-helium cannot be expressed as a simple function of film properties. This is due to the fact that in buoyancy driven flow, the velocity scale is not assigned independently but is intrinsically defined by the density difference between the condensing wall and the bulk. Basing on the McAdams correlation, the following relationship is obtained [7]

$$R_{LV} = \frac{\dot{m}_{v,i}''(h_2)}{\dot{m}_{v,i}''(he)} = \left(\frac{D_{vm}(h_2)}{D_{vm}(he)}\right)^{2/3} \left(\frac{\mu(h_2)}{\mu(he)}\right)^{-1/3} \left(\frac{\Delta \rho(h_2)}{\Delta \rho(he)}\right)^{1/3}$$

consisting of a film properties function, given by the product of density and viscosity ratios, and a function of density differences. Considering the same temperature conditions than the forced convection case, the comparison between the term  $R_{LV}$  and computational results is reported in Figure 14. The same phenomena described for helium tests must be expected, but *buoyancy* and *flow reversal* would occur in hydrogen tests for lower molar concentrations of the light gas, since hydrogen is lighter than helium.

## 5. Conclusions

Condensation phenomena in the presence of light noncondensable gases have been investigated. The synergy between experimental and computational analyses has allowed consolidating knowledge about forced and natural convection condensation, focusing on peculiar phenomena occurring in the presence of buoyancy effects. Indeed, a significant improvement has been

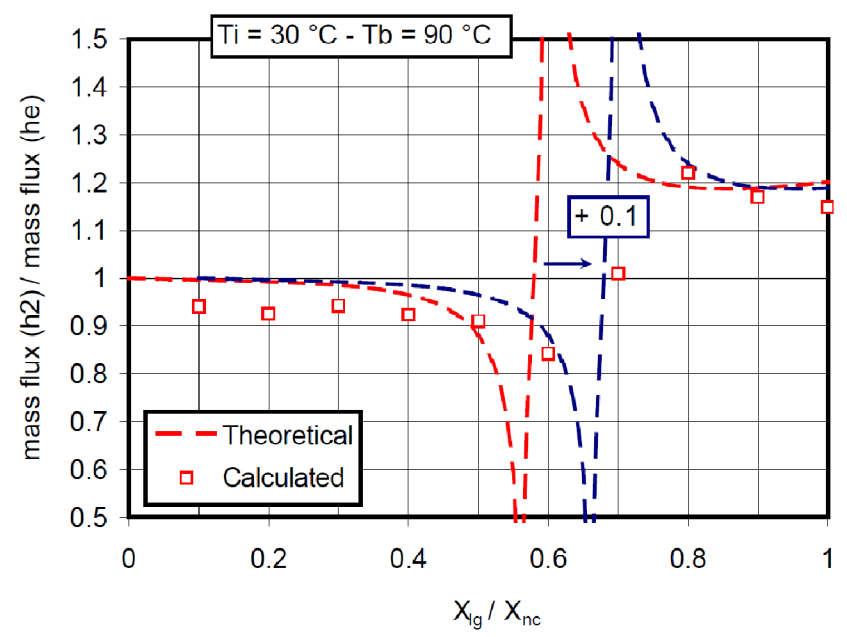


Figure 14 Comparison of theoretical and calculated  $R_{LV}$  at atmospheric pressure, 30 °C of condensation temperature and 90 °C of bulk temperature.

achieved in the understanding of *buoyancy* and *flow reversal* effects, made possible by simultaneous experimental and computational investigations.

Different CFD models have been developed and validated, adopting different modelling strategies and having different purposes. All models are capable to reproduce correctly the phenomena involved in steam-air-helium condensation tests, confirming also the reliability of experimental results. An experimental database is therefore made available, for the validation of codes. Finally, simple criteria for scaling of condensation tests in the presence of a light gas have been provided, demonstrating the suitability of helium as substitute for hydrogen and thus reinforcing the confidence in present and previous studies, and providing relevant guidelines for the design of future experimental investigations.

#### 6. Nomenclature

## Latin letters

Α	matrix of the MSD diffusion model	[-]
$B_m$	condensation driving force	[-]
D	diffusion coefficient	$[m^2/s]$
e	internal energy	[J/kg]
$\boldsymbol{F}$	Stefan suction factor	[-]
g	gravity acceleration	$[m/s^2]$
h	enthalpy	[J/kg]
$h_m$	mass transfer coefficient	$[kg/m^2/s]$
j	diffusion mass flux vector	$[kg/m^2/s]$
k	thermal conductivity	[W/m/K]
M	molecular weight	[kg/kmol]
$\dot{m}''$	condensation mass flux	$[kg/m^2/s]$

The 14<sup>th</sup> International Topical Meeting on Nuclear Reactor Thermalhydraulics, NURETH-14 Toronto, Ontario, Canada, September 25-30, 2011

		r 1
$\mathbf{n}_{\mathrm{i}}$	normal to the condensing interface	[-]
P	pressure	[Pa]
R	Scaling factor	[-]
R	matrix of the MSD diffusion model	[-]
S	scalar source term	$[-/m^3]$
S	vectorial source term	$[-/m^3]$
t	time	[s]
T	temperature	[K]
u	velocity vector	[m/s]
и	velocity module	[m/s]
Χ	molar fraction	[-]
x	spatial coordinate	[m]
Y	mass fraction	[-]

## Greek letters

α	thermal diffusivity	$[m^2/s]$
ε	turbulent kinetic energy dissipation	$[\text{m}^2/\text{s}^3]$
κ	turbulent kinetic energy	$[\text{m}^2/\text{s}^2]$
$\rho$	density	$[kg/m^3]$
$\mu$	dynamic viscosity	[Kg/s/m]
ν	kinematic viscosity	[Kg/s/m]
τ	shear stress tensor	[Pa]

# **Subscripts**

	C .	
а	refer to	21r
u	ICICI IO	an

c refer to the near-wall cell FC refer to forced convection

 $egin{array}{ll} h & ext{refer to enthalpy} \\ h_2 & ext{refer to hydrogen} \\ he & ext{refer to helium} \\ \end{array}$ 

*i* refer to the condensing interface

j refer to the species j
k refer to the species k
l refer to liquid
lg refer to the light gas
LV refer to low velocity

m refer to mass or mixture
 MC refer to mixed convection
 n refer to the species n

nc refer to noncondensablesNC refer to natural convectionp refer to the condensing plate

q refer to momentumt refer to turbulencev refer to vapour

0 refer to low mass transfer rate conditions

## Dimensionless numbers

$Re_x$	Reynolds number	$= \rho ux/\mu$
$Sh_{0,x}$	Sherwood number	$=h_{m,0}x/\rho D$
$Gr_x$	Sherwood number	$= \rho g \Delta \rho x^3 / \mu^2$
Sc	Schmidt number	= v/D
Pr	Prandtl number	$= v/\alpha$

#### 7. References

- [1] H.J. Allelein, K. Fischer et al., "International standard problem ISP-47 on containment thermal-hydraulics". Technical Report 10, OECD/NEA/CSNI, 2007.
- [2] W. Ambrosini, M. Bucci et al., "CFD models for predicting condensation in nuclear reactor containments within the SARnet network of excellence". Technical report, SARnet Report SARNET-CONT-P02, 2006.
- [3] W. Ambrosini, M. Bucci et al., "Comparison and Analysis of the Condensation Benchmark Results", Proceedings of the 3rd European Meeting on Severe Accident Research (ERMSAR-2008), 23-25 September, 2008, Nesseber, Bulgaria.
- [4] W. Ambrosini, M. Bucci et al., "CFD models for predicting condensation in nuclear reactor containments within the SARnet network of excellence". Technical report, SARnet Report SARNET-CONT-P02, 2006.
- [5] D. Lioce, "Prove sperimentali di condensazione di miscele ternarie di aria, elio-vapore e qualifica mediante un codice di CFD". Master's thesis, University of Pisa, 2006.
- [6] F. Poli, "Prove sperimentali sulla condensazione a film di miscele ternarie aria-elio-vapore e qualifica dei dati mediante un codice di CFD". Master's thesis, University of Pisa, 2007.
- [7] M. Bucci, "Experimental and computational analysis of steam condensation phenomena for the thermal-hydraulics analysis of LWRs containments". PhD thesis, University of Pisa, 2009.
- [8] M. Bucci, W.Ambrosini, E. Studer, "Theoretical and computational analysis of diffusion phenomena in condensing multicomponent mixtures". Submitted to Nuclear Engineering and Design, 2010.
- [9] R. Taylor and R. Kristhna, "Multicomponent Mass Transfer". Wiley, 1993.
- [10] H. Schlichting, "Boundary layer theory". McGraw-Hill, 1981.
- [11] F.P. Incropera, "Fundamentals of heat transfer". Wiley, 1965.
- [12] M. Bucci, E. Studer, J.P. Magnaud and W. Ambrosini, "Modelling of steam condensation phenomena in the presence of noncondensable gases: analysis of separate effect tests in forced, natural and mixed convection". Proceedings on the NURETH-13 conference. Kanazawa City, Ishikawa Prefecture, Japan, September 27-October 2, 2009.
- [13] Fluent Inc., "Fluent 6.2 user guide", Centerra Resource Park, Lebanon, NH., 2003.
- [14] M. Bucci, M. Sharabi, W. Ambrosini, N. Forgione, F. Oriolo, S. He, "Prediction of transpiration effects on heat and mass transfer by different turbulence models". Nuclear Engineering and Design, 238:958-974, 2008.
- [15] E. Deri, M. Turrin, M. Bucci, "Some consideration on the suitability of helium as a substitute for hydrogen in forced convection condensation experiments". Submitted to Nuclear Engineering and Design, 2011.